Biallelic mutation of *SUPV3L1* causes an inherited leukodystrophy-associated neurodevelopmental disorder due to aberrant mitochondrial double stranded RNA processing

Lydia Green[1,2ϕ], Noémie Hamilton[3,4ϕ], Marilena Elpidorou[2], Erica L. Harris[2], Andrew Douglas[5], Katrin Ounap[6], Reza Maroofian[7], Ailsa M.S. Rose[2], Stone Elworthy[3], Stephen A Renshaw[3], Elizabeth C. Low[3], Trine Prescott[8], Kristoffer Soberg[8], Almunder Al-Maawali[9], Sana Al-Zuhaibi[10], Amna Al Futaisi[11], Daniel Calame[12], Khalid Al-Thihli[9], Eamonn G. Sheridan[2], Colin A. Johnson[2], John Livingston[1], Yanick J. Crow[13], James A Poulter[2,*].

[1]Department of Paediatric Neurology, Leeds Teaching Hospitals Trust, Leeds, UK.

[2]Leeds Institute of Medical Research, University of Leeds, Leeds, UK.

[3]Bateson Centre, Department of Infection, Immunity and Cardiovascular Disease, University of Sheffield, Sheffield, UK.

[4]York Biomedical research Institute, Department of Biology, University of York, UK

[5]Oxford Centre for Genomic Medicine, Oxford, UK.

[6]Institute of Clinical Medicine and Department of Clinical Genetics, University of Tartu, Estonia.

[7]Department of Neuromuscular Disorders, University College London, London, UK

[8]Department of Clinical Genetics, Oslo University Hospital, Norway.

[9]Department of Genetics, College of Medicine and Health Sciences, Sultan Qaboos University Hospital, Sultan Qaboos University, Oman

[10]Ophthalmology Department, College of Medicine and Health Sciences, Sultan Qaboos University Hospital, Sultan Qaboos University, Oman

[11]Pediatric Neurology Unit, College of Medicine and Health Sciences, Sultan Qaboos University Hospital, Sultan Qaboos University, Oman.

[12]BCM-GREGoR Rare Disease Research Center, Baylor College of Medicine, US.

[13]Institute of Genetics and Cancer, MRC Human Genetics Unit, University of Edinburgh, Scotland, UK.

ϕ These authors contributed equally to this work.

*Corresponding author: Dr James A Poulter

University of Leeds

Wellcome Trust Brenner Building

Leeds Institute of Medical Research

St James' University Hospital

Beckett Street

Leeds LS9 7TF

UK

Email: J.A.Poulter@leeds.ac.uk

Abstract

Inherited white matter disorders (IWMD), or leukodystrophies (LD), are genetic disorders primarily affecting the white matter of the central nervous system (CNS), with or without peripheral nerve involvement. Recent developments in novel gene discovery has led to a greater understanding of myelin biology, with an increasing number of proteins with a wide variety of functions, involved in myelin development, maintenance and function. Here we describe 12 individuals from 9 families diagnosed with a neurodevelopmental disorder in whom biallelic variants in *SUPV3L1* have been identified. *SUPV3L1* encodes an RNA helicase with previous studies showing a key role in the mitochondrial degradosome. We found patient mutations led to an increase in mitochondrial double stranded RNAs in human cells and *supv3l1* knock-out zebrafish confirmed a role in neurodevelopment, with gross defects identified in mitochondrial biogenesis and microglial function. Zebrafish displayed a significant activation of the Type 1 interferon pathway, which was later also confirmed by qPCR on blood RNA from biallelic SUPV3L1 patients. Altogether we describe the clinical spectrum associated with biallelic *SUPV3L1* mutations and show the mutations identified result in increased mitochondrial double stranded RNA, altered mitochondrial biogenesis, dysplastic microglia and activation of the type 1 interferon innate immune pathway.

Introduction

Inherited white matter disorders (IWMD), or leukodystrophies (LD), are genetic disorders primarily affecting the white matter of the central nervous system (CNS), with or without peripheral nerve involvement. First described in the early 20th century [1], by 1980 the leukodystrophies were defined as progressive genetic disorders primarily affecting myelin and in the early 1990s a number of "classical leukodystrophies" had well described clinico-radiological phenotypes [2]. The late 20th century and advances in magnetic resonance imaging (MRI) techniques led to an exponential increase in the number of patients with radiologically confirmed LD, whose presentations were often heterogeneous and inconsistent with the classical LDs. This heterogeneous group, encompassing fatal neonatal diseases through to adult-onset motor disorders, alongside the recent revolution in genomic medicine led to the identification of several new LD and LD-associated genes. An example of this is seen in the expansion of the 173 gene IWMD panel within the UK's 100,000 genomes project (2013-2018) to the now 1,533 gene childhood white matter disorders super panel at the launch of Genomics England whole genome sequencing (WGS) service in 2021.

With the drive in novel gene discovery has come greater understanding of myelin biology and the identification of a wide range of proteins involved in its development, maintenance and function [3]. Increasingly represented are variants within genes encoding mitochondrial proteins, both within the nuclear and mitochondrial genomes. In a recent study of over 4000 LD patients, mutations in mitochondria associated genes accounted for approximately 5-10% of all LDs [4]. While many of these mutations were in genes encoding Complexes I-IV, mitochondria are not only essential for energy production, but also play a key role in regulation of cellular metabolism and proliferation.

Here we describe 12 individuals from 9 families identified with biallelic variants in mitochondrial RNA helicase gene *SUPV3L1*. SUPV3L1 has previously been shown to have a key role in the mitochondrial degradosome. Using a *SUPV3L1* complementation assay, we observed increased mitochondrial double-stranded RNA in the presence of patient mutations compared to wild-type *SUPV3L1*. Targeting *supv3l1 in vivo* in zebrafish resulted in reduced survival of fish with mitochondrial dysfunction. High resolution immune cell analysis identified abnormal microglia with an activated phenotype and a strong antiviral immune response signature in the brain. Altogether we show that biallelic mutations in *SUPV3L1* causes a spectrum of neurodevelopmental phenotypes resulting from the accumulation of mtdsRNA, activation of the innate immune system and disrupted mitochondrial dynamics.

Methods

Patient ascertainment

We included 12 patients from 9 unrelated families across 8 multinational institutions. Biallelic *SUPV3L1* variants were identified locally by next generation sequencing techniques following local procedures. GeneMatcher was used to identify biallelic *SUPV3L1* patients through an international collaboration [5]. Clinical and radiological data were retrospectively collected in Leeds and evaluated by an experienced paediatric neurologist (LG). The study was approved by the Yorkshire & Humber – Leeds East Research Ethics Committee (REC ref. 18/YH/0070). All patients and/or parents gave appropriate informed consent to be part of this study, and to be included in any publication, from their local institution in accordance with the principles outlined in the declaration of Helsinki. All patients underwent exome or genome sequencing as part of their local clinical care.

Molecular and Cellular Assays

Plasmid preparation and validation

Gene blocks of attB flanked SUPV3L1 containing each missense variant tested were obtained from Integrated DNA Technologies (Coralville, Iowa). Gene blocks were cloned into pDONR221 donor vector using the Gateway™ BP Clonase™ II Enzyme mix (ThermoFisher Scientific) and further cloned into the required destination vector using the Gateway™ LR Clonase™ II Enzyme mix (ThermoFisher Scientific) according to the manufacturers protocol. Sanger sequencing of the vectors confirmed the presence of each variant.

SUPV3L1 complementation assay

$2.5x10^5$ U2OS cells were seeded on to coverslips and 24 hours later transfected with a custom siRNA targeting the 5'UTR of *SUPV3L1* (Horizon technologies) using lipofectamine

RNAiMAX (ThermoFisher Scientific). 24 hours later, a second transfection was performed to introduce wild-type or variant-containing *SUPV3L1* using TransIT-X2 (Mirrus Bio). After 48 hours, U2OS cells were fixed with 4% para-formaldehyde. Following fixation, cells were permeabilised with 0.02% Triton X-100 for 5 minutes before washing with 1x phosphate-buffered saline (PBS) for a further 5 minutes. Wells were then blocked with 5% milk:PBS solution for 60 minutes at room temperature. Primary K1 anti-dsDNA antibody (Cell Signalling Technology) was prepared at a 1:500 dilution in a 3% milk:PBS solution and added to the wells for 60 minutes at room temperature. After three washes with PBS, cells were incubated with an Alexa Fluoro 488 anti-mouse secondary antibody (ThermoFisher Scientific, 1:500) and Hoescht (1:1,000). Secondary antibodies were prepared with 1% milk in PBS and incubated at room temperature, out of light, for 60 minutes. Once completed the cells were washed three times with PBS before mounting. Images were captured using a Niko A1R confocal microscope using NIS Elements software. ImageJ software was used to count dsRNA, using the SpotCounter plugin.

Zebrafish Modelling

Zebrafish husbandry and ethics

All zebrafish were raised in the Bateson Centre at the University of Sheffield in UK Home Office approved aquaria and maintained following standard protocols [6]. Tanks were maintained at 28°C with a continuous re-circulating water supply and a daily light/dark cycle of 14/10 hours. All procedures were performed under an animal Project Licence to standards set by the UK Home Office. We used the *Tg(mpeg1:mCherryCAAX)*sh378 labelling the membrane of macrophages and microglia [7] and the Tg(*AnnexinV*:mVenus)sh632 [8] to label dying cells.

Generation of supv3l1 zebrafish crispants

Synthetic SygRNA® consisting of gene specific CRISPR RNAs (crRNA) (Sigma) and transactivating RNAs (tracrRNA) (Merck) in combination with CAS9 nuclease protein (Merck) was used for gene editing. TracrRNA and crRNA were resuspended to a concentration of 100µM in nuclease free water containing 10mM Tris-HCl ph8. SygRNA® complexes were assembled on ice immediately before injection using a 1:1:1 ratio of crRNA:tracrRNA:Cas9 protein. We used the CHOPCHOP website [9] to design the following crRNA sequence specific to the zebrafish *supv3l1* gene (ENSDARG00000077728) targeting exon1, where the PAM site is indicated in brackets: GAAGACGCGGAGGGATCAGT(CGG). A 0.5nl drop of SygRNA®:Cas9 protein complex was injected into one-cell stage embryos. The resulting *supv3l1* crispants were used for the experiments, alongside a scrambled crRNA sequence for control group [10].

Construction of Tg(mpeg1.1:mts-mNeonGreen)sh631

The Tol2kit multisite Gateway method [11] was used with p5E-mpeg1.1 [12], pME-mts-mNeonGreen, p3E-polyA and pDestTol2pA2 [11] to create p(mpeg1.1:mts-mNeonGreen) transgene plasmid. The pME-mts-mNeonGreen middle-entry plasmid incorporated mts-mNeonGreen PCR amplified from a custom gBlock from IDT. The mts-mNeonGreen had the mitochondrial targeting sequence from zmLOC100282174 [13] as an N-terminal fusion to mNeonGreen (Shaner et al. 2013) via a (GGGGS)3 flexible linker and was codon optimised using CodonZ3 [14]. DNA sequencing confirmed the full transgene plasmid sequence (Core Genomics Facility University of Sheffield). The transgene plasmid was co-injected with tol2 transposase mRNA into Zebrafish embryos, the fish raised to adulthood and 3 day post fertilisation (dpf) larvae from outcrosses were screened for green fluorescent macrophages using a Zeiss Axio ZoomV16 microscope. Such F1 larvae were raised to adulthood and

screened by outcrossing. This identified the line sh631 that transmitted the transgene to 50% of progeny, indicating a single transgenic insertion.

Quantitative PCR

RNA was extracted from dissected heads of 5 day post fertilisation (dpf) zebrafish larvae using the Trizol/chloroform method. cDNA was synthetised using the SuperScript II kit (Invitrogen) with 2µg of RNA following manufacturer instructions and diluted in 1:20 for qPCR. qPCR primers were tested for efficiency (85%-105%) using a cDNA serial dilution. The qPCR reaction was run in a CFX96 Bio-Rad machine using validated primers as previously described [10]. Expression was normalised to *rpl13* as reference gene and relative to scrambled control set at 1.

Zebrafish confocal imaging and analysis

To assess microglial morphology, 5dpf scrambled and *supv3l1* crispant larvae injected in double reporter background *Tg(mpeg1:mCherryCAAX)*sh378 and Tg(*AnnexinV:mVenus*)sh632 were anaesthetised and embedded in low melting point agarose containing tricaine (0.168 mg/ml; Sigma-Aldrich) and imaged using a 40x objective on a UltraVIEW VoX spinning disk confocal microscope (PerkinElmer Life and Analytical Sciences). Z-stack were 100micron thick using 0.5µm slices. For microglial morphology analysis, sub-stacks of 50µm were used to create a maximum projection and contours of each microglia (avoiding pigment cells) were drawn using a pen tablet (Intuos from Wacom). Using Fiji, the circularity index (0-1) of each microglia was automatically recorded to assess the circularity of each cell with the value of 0 being not circular and 1 as being perfectly circular. To count the number of apoptotic cells, the same animals were imaged using the 10x lens on a UltraVIEW VoX spinning disk confocal microscope (PerkinElmer Life and Analytical

Sciences) using the brightfield alongside GFP and DsRed channels. Z- Stacks of 100µm with 2µm per slice were acquired and the brightfield image was used to draw a region of interest around the optic tectum as previously described [10].

TUNEL staining and quantification

Fish larvae at 5dpf were fixed in 4% PFA and the TUNEL assay was performed according to standard protocol using ApopTag Kit (Millipore) and as previously described [10]. Samples were imaged on the inverted W1 Nikon Spinning Disk confocal microscope using the brightfield and GFP channel by acquiring stacks of approximately 100µm with 2µm per slice. Using Fiji, the optic tectum region was outlined with the free hand drawing tool using the brightfield image and counting of number of apoptotic cells was performed using the automatic thresholding and particle count. All imaging analysis were blinded until after counting was performed.

Statistical analysis

All statistical analysis were performed in GraphPad Prism where data was entered using a column (2 samples, 1 variable only) spreadsheet. Sample distribution was assessed using frequency of distribution analysis and two-tailed Mann-Whitney U test was used for statistical analysis. All experiments were repeated using different batches of larvae born on different dates, with the number of biological replicates and n (experimental unit) number stated for each experiment in figure legends. p values are indicated and a star system is used instead for graph with multiple comparisons: *=$p<0.05$, **=$p<0.01$, ***=$p<0.001$, ****=$p<0.0001$. Following the recommendation of the American Statistical Association we do not associate a specific p value with significance [15].

Results

Through national and international collaborations, we identified twelve patients from nine families in whom biallelic *SUPV3L1* variants segregate with their disease phenotype (Figure 1A). Eleven different *SUPV3L1* variants were identified that were deemed to be likely pathogenic (CADD score > 15 and predicted damaging (PolyPhen2), deleterious (SIFT) or to impact splicing (SpliceAI)(Table 1). All variants are predicted to be loss of function with missense, frameshift, nonsense and splice site mutations identified. There was no apparent variant clustering, with variants distributed across the full length of the protein.

Biallelic *SUPV3L1* variants cause a variable neurodevelopmental syndrome

Detailed clinical characteristics are provided in Table S1. The age of onset was under 12 months in 11/12 patients, with patients presenting predominantly with developmental delay (n=7/12). Three patients presented prior to any noted delay, one in the antenatal period with abnormal antenatal scans, one at birth with neonatal thrombocytopenia and hypoglycaemia and one postnatally with feeding issues and weight loss. Other features at presentation included tonal abnormalities (spasticity 2/12, hypotonia 1/12), acquired microcephaly (1/12), areflexia (1/12), nystagmus (1/12) and ambiguous genitalia (1/12).

Overtime all patients developed developmental delay, being described as severe in 3 patients, and 11/12 intellectual disability. Two patients experienced developmental regression. 10 patients developed spasticity, 9 microcephaly, 4 epileptic seizures, 4 areas of skin depigmentation consistent with vitiligo, 2 movement disorders and 1 retinal dystrophy. 4 patients achieved walking, though only 1 independently between 1-3 years of age. The 3 others continue to require significant support aged between 5-13 years. At the time of writing 1 patient

was deceased – in addition to abnormal antenatal scans demonstrating lissencephaly, they also had respiratory distress syndrome, neonatal seizures and early spasticity.

From these clinical findings we see that *SUPV3L1* disorders present across a wide clinical spectrum from fatal neonatal disease through to infant-onset motor disorder with as-of-yet preserved cognition and ambulation. Most patients however demonstrate a progressive motor phenotype, and associated intellectual impairment is almost universal as is acquired microcephaly. Interestingly the reported skin hypopigmentation, reported in 4 of our patients, is also seen in 2 of the previously reported cases and is not a common feature of paediatric neurological disorders.

Dysmyelination and subcortical cysts in the temporal horn are a common feature of SUPV3L1-associated disease

From the 12 patients identified, MRI imaging was available for 6 patients. Detailed MRI findings are provided in Table S2. A number of features were observed in all available MRIs, including abnormal myelination, in particular dysmyelination, and subcortical cysts in the temporal horn. Additional features, such as cerebellar atrophy and a thin corpus callosum were observed in the majority of cases. P6 also showed calcifications in the basal ganglia, but these were not observed in any other patients.

SUPV3L1 variants do not cluster or map into any functional domain

SUPV3L1 is a mitochondrial double-stranded RNA (mtsdRNA) helicase. To determine if the variants identified clustered into any particular region or domain, we mapped all identified variants onto SUPV3L1 in 2D and 3D. Interestingly, we found most of the variants did not map onto any of the key functional domains of SUPV3l1, including the mitochondrial localisation

signal (amino acids (aa):1-21) the nucleotide binding domain (aa: 207-214) or the helicase domain (aa: 378-475)) (Figure 1B). Altogether this indicated that pathogenicity was not due to impairment of a particular function of SUPV3L1 (i.e. DNA binding or helicase activity).

SUPV3L1 mutations fail to rescue mtdsRNA levels following siRNA knockdown of *SUPV3L1*

As mapping of the variants provide little insight into the potential impact of the missense variants, we sought to confirm pathogenicity using a cell-based functional assay using dsRNA levels as a functional readout. We first created a custom siRNA mapping to the 3'-UTR of endogenous *SUPV3L1* and assessed the presence of mtdsRNA following transfection of the siRNA in U2OS cells. 48hrs after transfection of the siRNA, cells were fixed and immunofluorescence performed using a dsRNA antibody (K1). This revealed a significant increase in dsRNA compared to the non-targeting control (Suplementary Figure 1). To determine if this increase in dsRNA could be rescued by re-introduction of SUPV3L1, we co-transfected wild-type SUPV3L1 with the custom siRNA and assessed levels of dsRNA. We observed a significant decrease in dsRNA in cells co-transfected with siRNA and SUPV3L1^{WT} compared to siRNA alone, consistent with a rescue of the phenotype. We subsequently introduced all variants with conflicting pathogenicity scores from PolyPhen2 and SIFT analysis into the WT SUPV3L1 and assessed their ability to rescue the increase in dsRNA following siRNA induced knockdown of SUPV3L1. For all missense variants tested, we observed no rescue of the increased dsRNA levels as observed with transfection of SUPV3L1^{WT}, indicating that all variants have an impact on protein function and likely account for disease.

Loss of *supv3l1* in a zebrafish model results in immune dysfunction and activation of antiviral immune pathway.

Using the highly efficient CRISPR/Cas9 gene targeting system, we generated a *supv3l1* crispant and used the previously published survival and mitochondrial phenotype [16] to assess efficiency of the CRISPR/Cas9 complex targeting the *supv3l1* gene. Injected embryos with *supv3l1* crRNA showed reduced survival compared to scrambled control injected and had to be humanely culled by 8dpf due to signs of necrosis in the liver, lack of swimming and deflated swim bladder (Figure 2A,B). Mitochondrial dysfunction was confirmed using a novel reporter line Tg(*mpeg1*:mls-neon)sh631 labelling mitochondria in the macrophage/microglia lineage with significantly more microglia displaying mitochondria fusion and fission in *supv3l1* crispants (Figure 2C-E).

To analyse the effect of dysfunctional mitochondria in microglia and the wider brain, 5dpf zebrafish were live imaged at high resolution to measure microglial morphology and cell death in the optic tectum region, using the Tg(*mpeg1*:mCherryCAAX)sh378 and Tg(*AnnexinV*:mVenus)sh632 reporter lines respectively. Microglia in 5dpf brains of *supv3l1* crispants displayed an activated phenotype, with rounder cell body measured using FiJi circularity index (Figure 3A-B,D) and showed an intriguing membrane ruffled phenotype (Figure 3B- high magnification panel). Using the Tg(*AnnexinV*:mVenus)sh632 reporter line to label apoptotic cells, we counted a higher number of apoptotic cells in *supv3l1* crispant brains, which was confirmed using the traditional TUNEL staining (Figure 3E,F).

To assess the neuroinflammatory state of the brain, we extracted RNA from 5dpf zebrafish heads of *supv3l1* and control and performed qPCR using a panel of inflammatory genes (Figure 3G,H). We identified a more than 400-fold upregulation of expression for genes specific to the antiviral immune pathway, such as the human orthologue of IFN-1 called *ifnΦ1* [17] and interferon-induced genes such as *isg15* and *mxa* (Figure 3H). Activation of the antiviral

immune response was confirmed using a reporter line for the *mxa* gene Tg(*cryaa*:Dsred;*mxa*:mCherryF)ump7tg highlighting a systemic activation of the antiviral immune pathway (Figure 3I).

Discussion

Through an international collaboration, we have identified 12 patients from 9 families in whom biallelic SUPV3L1 variants segregate with disease and identify common phenotypes across all patients including abnormal myelination and subcortical cysts in the temporal horn. Of interest, we observed skin hypopigmentation in 4 of our patients, which was also seen in 2 of the previously reported cases. Skin hypopigmentation, also referred to as vitiligo, is not a common feature of paediatric neurological disorders and therefore we suggest SUPV3L1 sequencing should be prioritised in individuals presenting with a neurodevelopmental disorder and vitiligo. We further demonstrate the impact of biallelic SUPV3L1 variants on levels of double stranded RNA and show loss of *supv3l1* in a zebrafish model results in defects in mitochondrial biogenesis and activation of the innate immune response.

Dawidziuk *et al* reported the first probable cases of *SUPV3L1* causing human disease in a pair of siblings with microcephaly, one of whom had white matter changes [18]. These were identified from a cohort of patients with congenital microcephaly who underwent WES and no other candidate variants were identified. Van Esveld *et al.* reported a further two cases where *SUPV3L1* variants were confirmed to cause a neurodegenerative presentation in a sibling pair, with a family history of two other affected siblings and an affected cousin for whom samples were not available for testing [19]. The siblings were homozygous for the same c.2215C>T, p.Gln739* variant identified in two families (F6 and F7), both of which were identified through a larger screen of intellectual disability patients from the Middle East [20]. The phenotype described by van Esveld and colleagues was a progressive spastic paraparesis with growth restriction, hypopigmentation and a predisposition to autoimmune disease, all features observed across the patients described in this study [19]. One of the siblings also demonstrated

subtle white matter changes in the form of focal areas of T2 hyperintensity as well as some delayed myelination.

Mapping of the variants on the SUPV3L1 protein revealed no clustering, with all variant types found across the full length of the protein. The p.Gln739Ter nonsense variant is located in the final exon of *SUPV3L1* and therefore is expected to escape nonsense mediated decay and form a truncated protein which may retain some function. Van Esveld investigated the same p.Gln39Ter variant in patient cells by Western blot and showed the truncated protein was present, albeit at a reduced levels [19]. This is consistent with previous studies which found complete knockout of *SUPV3L1* results in embryonic lethality [21] and may suggest that all variants identified in *SUPV3L1* in humans are hypomorphic, with some retained function. A frameshift variant was also identified, which would be predicted to lead to loss of protein, however this variant was identified to be compound heterozygous with the missense variant p.Ser642Arg which may retain some function due to its location outside of any functional domain. Mapping of the missense variants showed only 2/7 were present in a functional domain. Both of these variants, p.Alal393Thr and p.Pro414Ser, are located in the helicase domain and may therefore directly impact helicase activity. The remaining variants are located outside of the functional domains suggesting a potential impact on the overall structure of SUPV3L1. Indeed, analysis of the 3D crystal structure of SUPV3L1 shows Arg-365 forms an interaction with Glu-482, therefore the homozygous p.Arg365Trp substitution identified in P1 is likely to result in the loss of this charged interaction and an impact on overall protein structure. To date, no variants in SUPV3L1 have been identified in the mitochondrial signal peptide nor in the nucleotide binding domain. Further work is required to further delineate the effect of the mutations identified on SUPV3L1 function.

Helicases are highly conserved motor proteins with a role in almost all nucleic acid metabolic processes including replication, repair and degradation [22]. First discovered in yeast in 1992 *SUPV3L1* encodes an ATP-dependent RNA/DNA helicase that, when bound to polyribonucleotide nucleotidyltransferase 1 (PNPT1 or PNPase), forms an essential part of the human mitochondrial degradosome [23]. Preferentially located within the mitochondria, but with some cytosolic presence, the SUPV3L1-PNPase complex is responsible for unwinding aberrant or unwanted dsRNA, dsDNA and RNA:DNA hybrids in a 3'-5' direction [24]. Maintaining effective turnover of unwanted nucleic acid material is critical for mitochondrial health and function. Supv3l1 knockout in mice results in embryonic lethality, with further investigations identifying a role for SUPV3L1 in the cytoplasm to suppress mitotic homologous recombination [21]. A gene trap *supv3l1* zebrafish mutant showed mitochondrial dysfunction, impaired liver development and reduced survival therefore confirming a conserved role for SUPV3L1 in vertebrate in mitochondrial homeostasis [16]. Altogether this indicates *SUPV3L1* to be an essential gene with potential housekeeping function however its role in the brain and the maintenance of white matter is currently unknown.

The development of animal models to study neurodevelopmental disorders, including leukodystrophies, *in vivo* has been invaluable for testing therapies [25-28], however many of those rodent models fail to recapitulate the key aspects of the human disease or are embryonic lethal [29]. A homozygous *Supv3l1* mutation in mice results in embryonic lethality but showed a role for SUPV3L1 in the cytoplasm to suppress mitotic homologous recombination [21]. Zebrafish have been used successfully to model neurodevelopmental disorders due to its ex-utero transparent development, allowing real time analysis of cellular events during brain development [10, 30-34]. The zebrafish brain is fully developed by 8dpf with a structure and development similar to other vertebrate including chicken, rat and human [35, 36]. In this

study, we targeted the orthologous *supv3l1* gene using CRISPR/Cas9, generating an *in vivo* zebrafish model that recapitulated the previous published phenotype made using a gene trap system [16]. Loss of *supv3l1* in zebrafish resulted in reduced survival with most injected crispants requiring humane culling by 8dpf. Immune cell analysis in the brain identified abnormal microglia with an activated phenotype and a strong antiviral immune response signature in the brain at 5dpf.

Considering all of the above evidence on SUPV3L1 function, there was some justification as to how this candidate gene could potentially affect growth and development as seen in the families identified in this study. In addition, as a protein localised in the mitochondria, SUPV3L1 could be interacting with other key proteins that have been shown to be involved in developmental disorders, specifically with white matter abnormalities. In particular, SUPV3L1 is known to interact with PNPT1, an RNA binding protein involved in RNA metabolism and a component of the mitochondrial RNA degradosome. The mitochondrial RNA degradosome complex is a heteropentamer consisting of a PNPT1 trimer and a SUPV3L1 dimer, that in yeast has been demonstrated to degrade double-stranded RNA in the presence of ATP [24]. If one of the two components of the heteropentamer is disrupted, the activity of the degradosome is abolished. Of note, biallelic variants in *PNPT1* are also shown to be associated with abnormal myelination in patients with neurodevelopmental disease and mitochondrial dysfunction [37]. This association provides additional evidence that pathogenic variants in genes encoding components of the mitochondrial degradosome result in neurodevelopmental disorders characterised by defects in mtdsRNA processing and subsequently mitochondrial function.

In summary, we have identified 12 patients with a neurodevelopmental disorder in whom biallelic *SUPV3L1* variants segregate with disease. We identified abnormal myelination and

subcortical cysts in the temporal horn to be common features as well as hypopigmentation of the skin, consistent with vitiligo – a rare co-occurrence with neurodevelopmental disorders. We found the variants identified failed to reduce mtdsRNA levels in a complementation assay and modelling of supv3l1 loss in fish showed significant effects on mitochondrial biogenesis and microglial function with a systemic activation of the antiviral immune pathway.

Acknowledgements

The authors would like to thank the family and the patients for participating in this study. The study was funded by a Sir Jules Thorn Award for Biomedical Research (JTA/09 to E.G.S and C.A.J.), a University of Leeds Academic Fellowship (to J.A.P), a University of Leeds PhD studentship (to M.E) and a White Rose Universities Collaboration grant (to N.H. and J.A.P). J.A.P is supported by a UKRI Future Leaders Fellowship (MR/T02044X/1). N.H. is supported by a grant from The Legacy of Angels. S.A.R is supported by a Medical Research Council grant to SHIELD consortium MR/NO2995X/1. The research is supported by the National Institute for Health Research (NIHR) infrastructure at Leeds. The views expressed are those of the author(s) and not necessarily those of the NHS, the NIHR or the Department of Health.

Author Contributions

Project administration: J.A.P, N.H, C.A.J; Conceptualisation: J.A.P, N.H, S.A.R, Y.J.C; Funding Acquisition: J.A.P, N.H, S.A.R, C.A.J, E.G.S; Resources: N.H, S.A.R, J.A.P; Patient care: L.G, A.D, K.O, T.P, K.S, A.A, S.A, A.A.F, D.C, K.A, E.G.S, J.L, Y.J.C; Genetic Analysis and data collection: M.E, E.L.H, R.M, A.M.S.R, E.C.L; Methodology: N.H, S.E, J.A.P; Supervision: J.A.P, N.H, S.A.R, C.A.J, E.G.S,, Y.J.C; Writing Original draft: L.G, N.H, J.A.P. All authors read an approved the final manuscript.

Data Availability

The datasets generated and analysed during the current study are available from the corresponding author on reasonable request.

Conflict of interest

The authors declare that they do not identify any competing interests.

REFERENCES

1. Nissl, F. and A. Alzheimer, *Histologische und histopathologische Arbeiten über die Grosshirnrinde: mit besonderer Berücksichtigung der pathologischen Anatomie der Geisteskrankheiten*. 1910: G. Fischer.
2. Aicardi, J., *The inherited leukodystrophies: a clinical overview.* J Inherit Metab Dis, 1993. **16**(4): p. 733-43.
3. Wolf, N.I., C. Ffrench-Constant, and M.S. van der Knaap, *Hypomyelinating leukodystrophies - unravelling myelin biology.* Nat Rev Neurol, 2021. **17**(2): p. 88-103.
4. Roosendaal, S.D., et al., *Imaging Patterns Characterizing Mitochondrial Leukodystrophies.* AJNR Am J Neuroradiol, 2021. **42**(7): p. 1334-1340.
5. Sobreira, N., et al., *GeneMatcher: a matching tool for connecting investigators with an interest in the same gene.* Hum Mutat, 2015. **36**(10): p. 928-30.
6. NÜSSLEIN-VOLHARD, C. and R. DAHM, eds. *Zebrafish: A Practical Approach*. 2003, Oxford University Press. 322.
7. Bojarczuk, A., et al., *Cryptococcus neoformans Intracellular Proliferation and Capsule Size Determines Early Macrophage Control of Infection.* Sci Rep, 2016. **6**: p. 21489.
8. Kugler, E., et al., *The effect of absent blood flow on the zebrafish cerebral and trunk vasculature.* Vasc Biol, 2021. **3**(1): p. 1-16.
9. Labun, K., et al., *CHOPCHOP v3: expanding the CRISPR web toolbox beyond genome editing.* Nucleic Acids Res, 2019. **47**(W1): p. W171-W174.
10. Hamilton, N., et al., *The failure of microglia to digest developmental apoptotic cells contributes to the pathology of RNASET2-deficient leukoencephalopathy.* Glia, 2020. **68**(7): p. 1531-1545.

11. Kwan, K.M., et al., *The Tol2kit: a multisite gateway-based construction kit for Tol2 transposon transgenesis constructs.* Dev Dyn, 2007. **236**(11): p. 3088-99.

12. Ellett, F., et al., *mpeg1 promoter transgenes direct macrophage-lineage expression in zebrafish.* Blood, 2011. **117**(4): p. e49-56.

13. Chin, R.M., et al., *Optimized Mitochondrial Targeting of Proteins Encoded by Modified mRNAs Rescues Cells Harboring Mutations in mtATP6.* Cell Rep, 2018. **22**(11): p. 2818-2826.

14. Horstick, E.J., et al., *Increased functional protein expression using nucleotide sequence features enriched in highly expressed genes in zebrafish.* Nucleic Acids Res, 2015. **43**(7): p. e48.

15. Wasserstein, R.L., A.L. Schirm, and N.A. Lazar, *Moving to a World Beyond "p < 0.05".* The American Statistician, 2019. **73**(sup1): p. 1-19.

16. Ni, T.T., et al., *Conditional control of gene function by an invertible gene trap in zebrafish.* Proc Natl Acad Sci U S A, 2012. **109**(38): p. 15389-94.

17. Boudinot, P., et al., *The Peculiar Characteristics of Fish Type I Interferons.* Viruses, 2016. **8**(11).

18. Dawidziuk, M., et al., *Exome Sequencing Reveals Novel Variants and Expands the Genetic Landscape for Congenital Microcephaly.* Genes (Basel), 2021. **12**(12).

19. van Esveld, S.L., et al., *Mitochondrial RNA processing defect caused by a SUPV3L1 mutation in two siblings with a novel neurodegenerative syndrome.* J Inherit Metab Dis, 2022. **45**(2): p. 292-307.

20. Al-Kasbi, G., et al., *The diagnostic yield, candidate genes, and pitfalls for a genetic study of intellectual disability in 118 middle eastern families.* Sci Rep, 2022. **12**(1): p. 18862.

21. Pereira, M., et al., *Interaction of human SUV3 RNA/DNA helicase with BLM helicase; loss of the SUV3 gene results in mouse embryonic lethality.* Mech Ageing Dev, 2007. **128**(11-12): p. 609-17.

22. Raney, K.D., A.K. Byrd, and S. Aarattuthodiyil, *Structure and Mechanisms of SF1 DNA Helicases.* Adv Exp Med Biol, 2013. **767**: p. 17-46.

23. Stepien, P.P., et al., *The yeast nuclear gene suv3 affecting mitochondrial post-transcriptional processes encodes a putative ATP-dependent RNA helicase.* Proc Natl Acad Sci U S A, 1992. **89**(15): p. 6813-7.

24. Wang, D.D., et al., *Human mitochondrial SUV3 and polynucleotide phosphorylase form a 330-kDa heteropentamer to cooperatively degrade double-stranded RNA with a 3'-to-5' directionality.* J Biol Chem, 2009. **284**(31): p. 20812-21.

25. Biffi, A., et al., *Correction of metachromatic leukodystrophy in the mouse model by transplantation of genetically modified hematopoietic stem cells.* J Clin Invest, 2004. **113**(8): p. 1118-29.

26. Marshall, M.S., et al., *Long-Term Improvement of Neurological Signs and Metabolic Dysfunction in a Mouse Model of Krabbe's Disease after Global Gene Therapy.* Mol Ther, 2018. **26**(3): p. 874-889.

27. Priller, J., et al., *Targeting gene-modified hematopoietic cells to the central nervous system: use of green fluorescent protein uncovers microglial engraftment.* Nat Med, 2001. **7**(12): p. 1356-61.

28. Adamson, K.I., E. Sheridan, and A.J. Grierson, *Use of zebrafish models to investigate rare human disease.* J Med Genet, 2018. **55**(10): p. 641-649.

29. Rutherford, H.A. and N. Hamilton, *Animal models of leukodystrophy: a new perspective for the development of therapies.* FEBS J, 2019. **286**(21): p. 4176-4191.

30. Haud, N., et al., *rnaset2 mutant zebrafish model familial cystic leukoencephalopathy and reveal a role for RNase T2 in degrading ribosomal RNA.* Proc Natl Acad Sci U S A, 2011. **108**(3): p. 1099-103.

31. Kasher, P.R., et al., *Characterization of samhd1 morphant zebrafish recapitulates features of the human type I interferonopathy Aicardi-Goutieres syndrome.* J Immunol, 2015. **194**(6): p. 2819-25.

32. Oosterhof, N., et al., *Homozygous Mutations in CSF1R Cause a Pediatric-Onset Leukoencephalopathy and Can Result in Congenital Absence of Microglia.* Am J Hum Genet, 2019. **104**(5): p. 936-947.

33. Pant, D.C., et al., *Loss of the sphingolipid desaturase DEGS1 causes hypomyelinating leukodystrophy.* J Clin Invest, 2019. **129**(3): p. 1240-1256.

34. Strachan, L.R., et al., *A zebrafish model of X-linked adrenoleukodystrophy recapitulates key disease features and demonstrates a developmental requirement for abcd1 in oligodendrocyte patterning and myelination.* Hum Mol Genet, 2017. **26**(18): p. 3600-3614.

35. Lowery, L.A. and H. Sive, *Strategies of vertebrate neurulation and a re-evaluation of teleost neural tube formation.* Mech Dev, 2004. **121**(10): p. 1189-97.

36. Tropepe, V. and H.L. Sive, *Can zebrafish be used as a model to study the neurodevelopmental causes of autism?* Genes Brain Behav, 2003. **2**(5): p. 268-81.

37. Sato, R., et al., *Novel biallelic mutations in the PNPT1 gene encoding a mitochondrial-RNA-import protein PNPase cause delayed myelination.* Clin Genet, 2018. **93**(2): p. 242-247.

Table 1 – Summary of variants identified in SUPV3L1.

DNA variant	Protein variant	dbSNP: rs number	gnomAD Frequency	PolyPhen2	SIFT	CADD (v1.6)	SpliceAI	Family
c.196C>T	p.Pro66Leu	rs752705209	$5.6x10^{-5}$ (14/250,924)	Prob. Dam. 1.00	DEL 0.00	32.0	0.00	9*
c.329G>A	p.Gly110Asp	Not Present	Not Present	Benign 0.082	DEL 0.00	22.5	0.00	5
c.458-2A>G	p.(splice)	Not Present	Not Present	N/A	N/A	34.0	0.99 (Acc.L)	2*
c.854-3A>G	p.(splice)	Not Present	Not Present	N/A	N/A	17.61	0.50 (Acc.L)	4
c.1093C>T	p.Arg365Trp	rs527626577	$1.8x10^{-5}$ (5/282,676)	Poss. Dam. 0.462	DEL 0.00	31.0	0.00	1
c.1070C>A	p.Ala357Glu	Not Present	Not Present	Prob. Dam. 0.957	DEL 0.00	25.4	0.00	2*
c.1177G>A	p.Ala393Thr	rs1025320000	$8.0x10^{-6}$ (2/251,320)	Prob. Dam. 0.934	TOL 0.05	25.7	0.01 (Don.G)	8
c.1240C>T	p.Pro414Ser	Not Present	Not Present	Prob. Dam 0.967	DEL 0.00	25.4	0.00	9*
c.1321dup	p.Tyr441Leufs*10	Not Present	Not Present	N/A	N/A		0.00	3*
c.1924A>C	p.Ser642Arg	rs750670256	$8.0x10^{-6}$ (2/249,812)	Prob. Dam. 0.999	DEL 0.00	33.0	0.02 (Don.L)	3*
c.2215C>T	p.Gln739Ter	Not Present	Not Present	N/A	N/A	39.0	0.00	6, 7

Variant nomenclature based on transcript ENST00000359655.4. * Signifies a compound heterozygous variant.
Abbreviations. **PolyPhen2:** Prob.Dam, Probably Damaging; Poss. Dam., Possibly Damaging. **SIFT:** DEL, Deleterious; TOL, Tolerated. **SpliceAI;** Acc.L, Acceptor Loss; Don.G, Donor Gain; Don.L, Donor Loss.

Figures and Legends

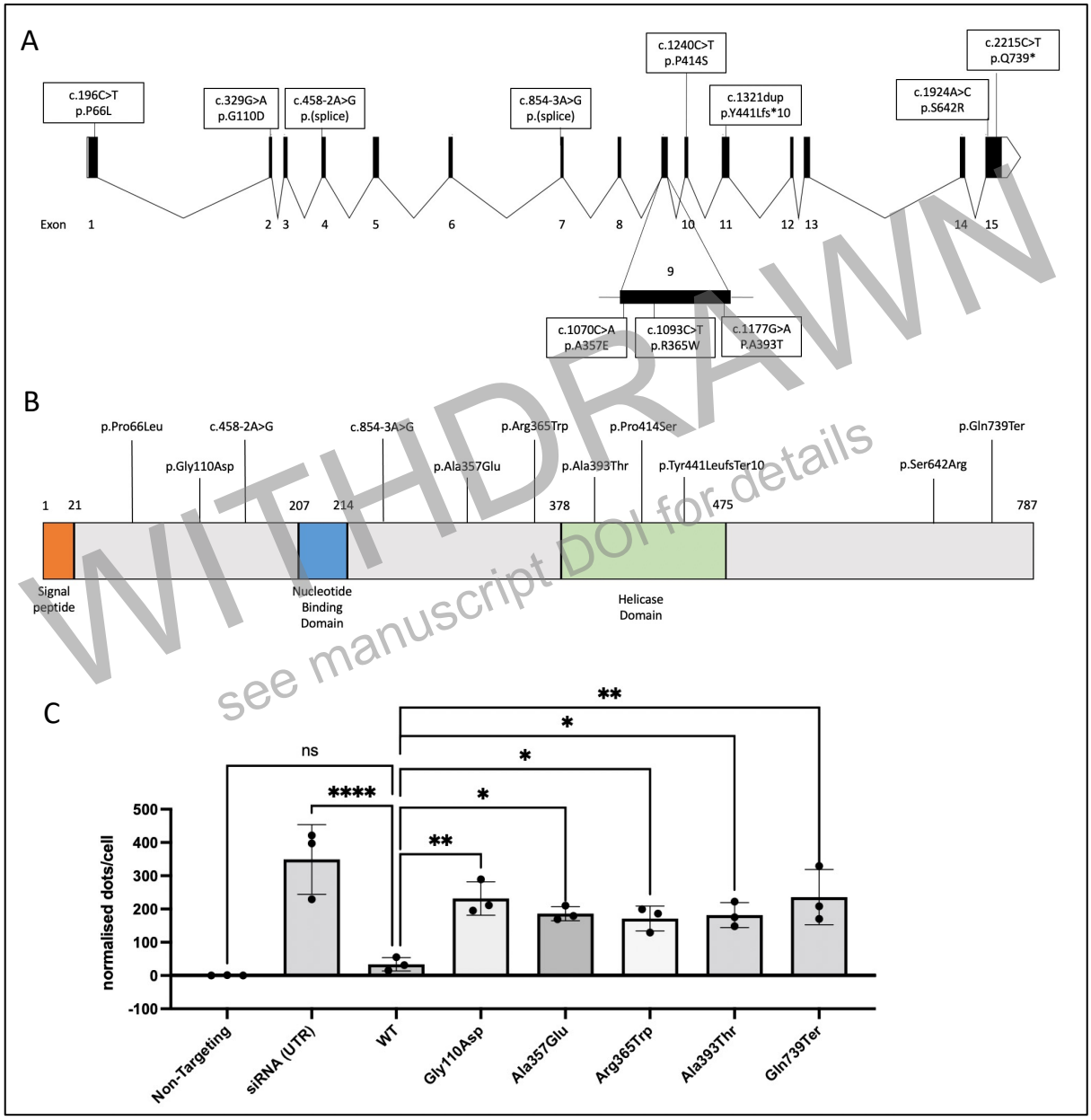

Figure 1 – Genetic and proteomic mapping of pathogenic SUPV3L1 variants.
A. Schematic of the 15 exons and introns of human *SUPV3L1* annotated with the 11 different variants identified in this study**. B.** Schematic of the SUPV3L1 protein showing the location of variants relative to the known protein domains. **C.** Summary of complementation assay performed on all variants of unknown significance. All missense variants identified failed to reduce the number of mtdsRNA to the levels of the wildtype, confirming an effect on SUPV3L1 function.

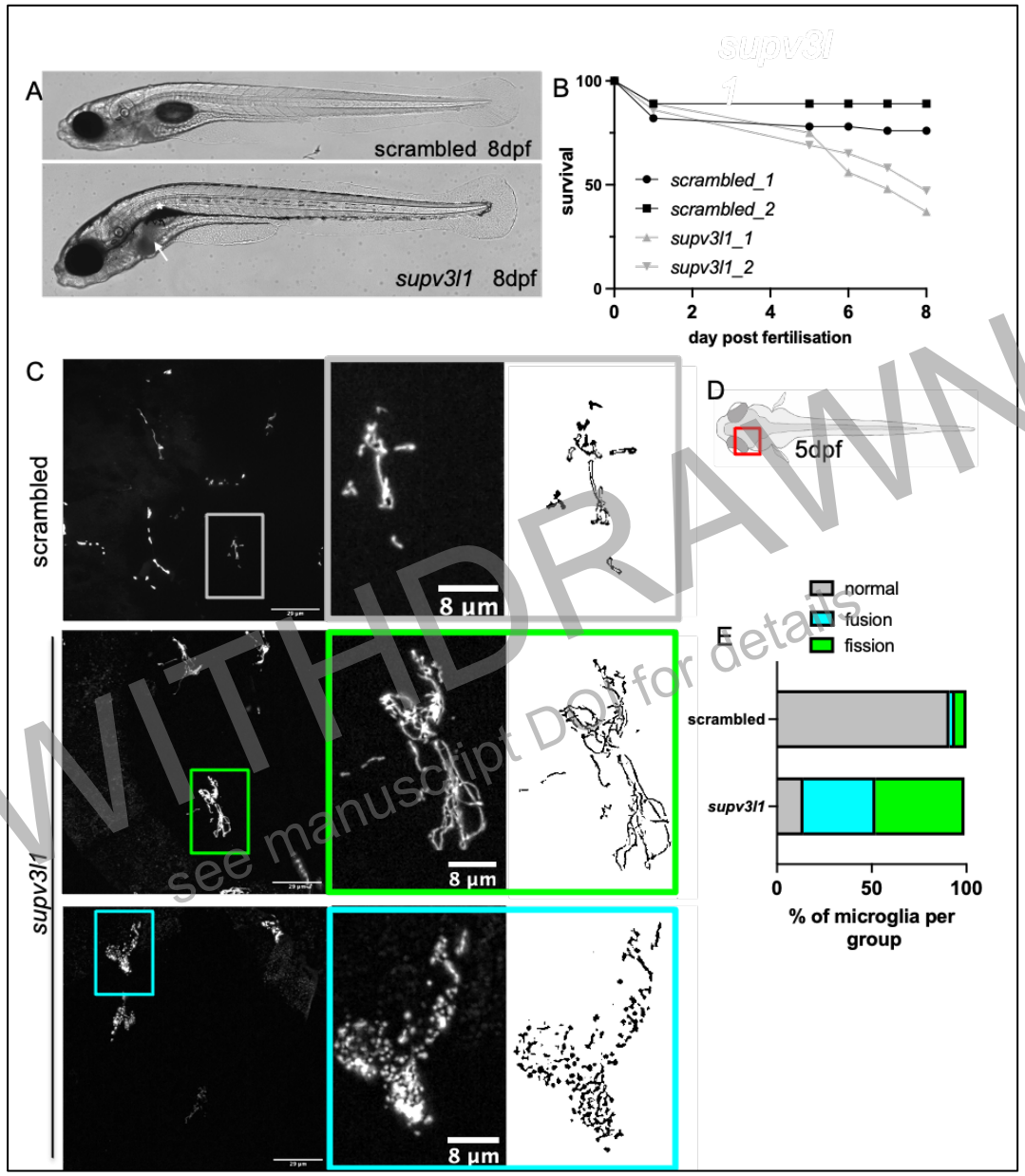

Figure 2: Loss of *supv3l1* in zebrafish decreases survival and induces mitochondrial stress
A. Representative brightfield images of 8dpf zebrafish larvae injected with scrambled control and *supv3l1* crRNA. Note the necrotic liver (white arrow) and deflated swim bladder (white asterisk) in *supv3l1* injected larvae as previously reported in *supv3l1* mutant.
B. Survival analysis of scrambled control and *supv3l1* crRNA injected larvae until 8dpf. Death outcome is represented by humanely culling animals displaying an emaciated phenotype.
C. Representative confocal images of 5dpf zebrafish brains from scrambled control and *supv3l1* crRNA injected larvae in the macrophage-specific mitochondria reporter line Tg(mpeg1:mls-neon)sh631. Scale bar 29µm. High magnification image of a microglia selected from the coloured rectangle and associated Mask image generated in FiJi using the '**T**ubeness' plugins. Scale bar 8µm.
D. Diagram of a dorsal view of a 5dpf zebrafish head with red box highlighting the region imaged and the transgenic lines used in panel C.
E. Quantification of number of microglia displaying a normal, fusion **or fission** mitochondria phenotype in the optic tectum. N=12-14 from 2 independent experiments, using Chi-square test from contingency table (****: p<0.0001).

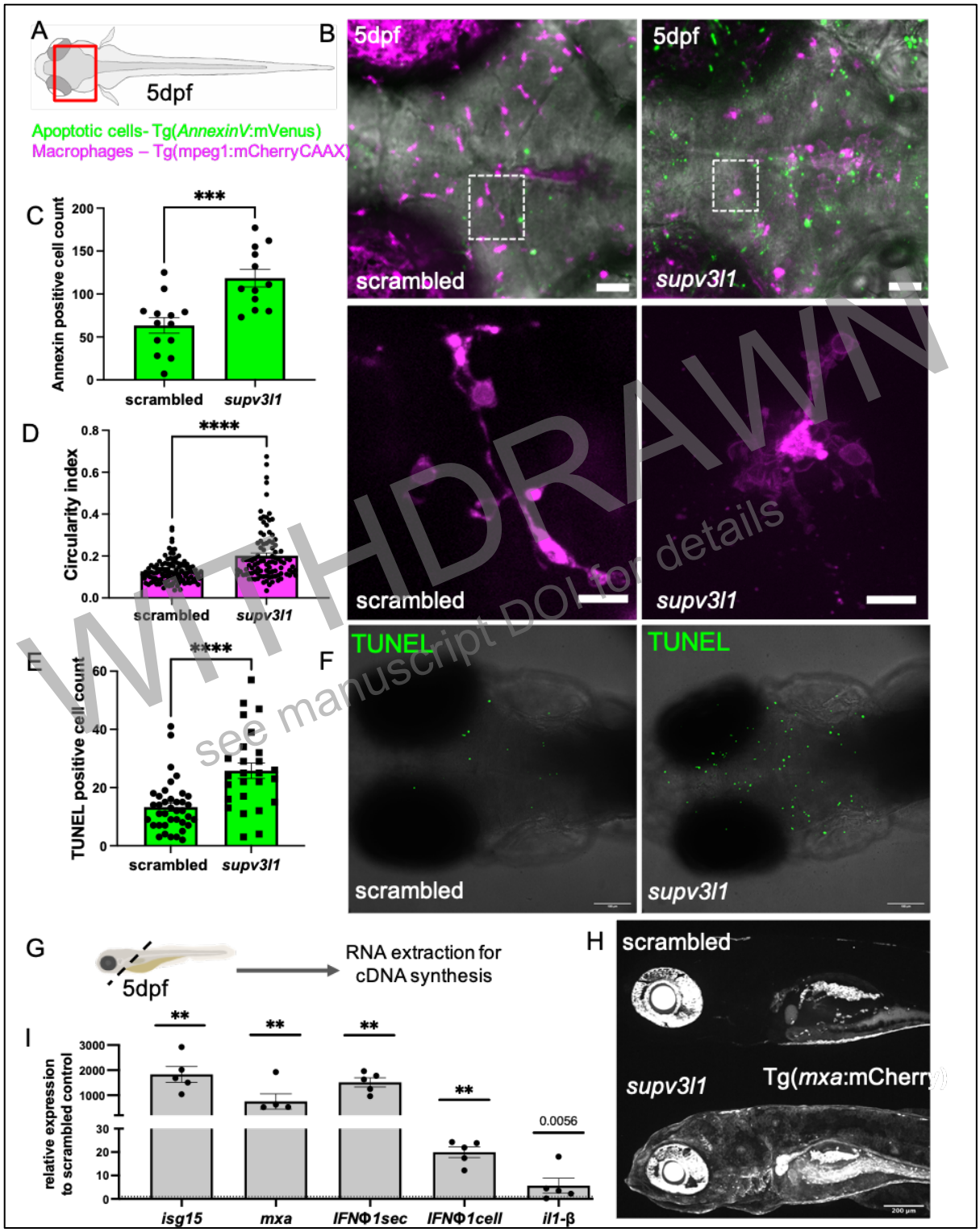

Figure 3: Loss of supv3l1 activates microglia and triggers systemic antiviral immunity activation.

A. Diagram of a dorsal view of a 5dpf zebrafish head with red box highlighting the region imaged and the transgenic lines used in panel F.

B. Representative confocal images of 5dpf zebrafish brains from scrambled control and *supv3l1* crRNA injected larvae in the double Tg(*AnnexinV*:mVenus)sh632;Tg(*mpeg1*:mCherryCAAX)sh378 background, labeling

apoptotic cells and macrophages respectively. Scale bar 50µm. High magnification image of a macrophage selected from the dotted rectangle. Scale bar 10µm.

C. Quantification of Annexin positive apoptotic cells in the optic tectum. n=12-13 from 2 independent experiments, using two-tailed Mann-Whitney U test (***: $p<0.001$).

D. Quantification of macrophages circularity measuring the circularity index using the Tg(*mpeg1*:mCherryCAAX)sh378 reporter line. n=98-115 macrophages from 3 independent experiments, using two-tailed Mann-Whitney U test (****: $p<0.0001$).

E. Quantification of TUNEL positive apoptotic cells in the optic tectum. n=26-38 from 3 independent experiments, using two-tailed Mann-Whitney U test (****: $p<0.0001$).

F. Representative confocal images of 5dpf zebrafish brains from scrambled control and *supv3l1* crRNA injected larvae and stained for apoptotic cells using TUNEL staining. Scale bar 100µm.

G. Diagram of experimental setup to analysis gene expression from zebrafish brain by qPCR

H. qPCR analysis of antiviral genes *mxa*, *isg15*, ifnΦ1secreted and cellular, and inflammatory gene *il1-beta* from heads of 5dpf scrambled control and *supv3l1* crRNA injected larvae. Expression relative to scrambled control set at 1 (dotted line) and normalised to *rpl13* reference gene. n=5 from 5 independent experiments, two-tailed Mann-Whitney U test, p value shown on individual graphs.

I. Representative confocal images of 5dpf zebrafish from scrambled control and *supv3l1* crRNA injected larvae in the Tg(cryaa:Dsred;mxa:mCherryF)^{ump7tg} reporter line. Scale bar 200µm.

Supplementary Data

Supplementary Table 1: Clinical characteristics of the 12 patients with biallelic *SUPV3L1* variants.

Supplementary Table 2: MRI features of patients with *SUPV3L1* variants.

Supplementary Figure 1 – representative images from the optimisation and validation of the dsRNA complementation assay.

Supplementary Table 1: Clinical characteristics of the 12 patients with biallelic *SUPV3L1* variants

	Family 1			**Family 2**	**Family 3**
	P1	**P2**	**P3**	**P4**	**P5**
Variant 1; Variant 2	c.1093C>T, p.Arg365Trp; c.1093C>T, p.Arg365Trp	c.1093C>T, p.Arg365Trp; c.1093C>T, p.Arg365Trp	c.1093C>T, p.Arg365Trp; c.1093C>T, p.Arg365Trp	c.458-2A>G, p.(splice); c.1070C>A, p.Ala357Glu	c.1321dup, p.Tyr441Leufs*10; c.1924A>C, p.Ser642Arg
Presentation Age at onset Presenting features	 Infant Developmental delay, hypotonia	 Infant Developmental delay, hypotonia	 Unk Speech and motor delay	 Infant Feeding issues, weight loss	 Infant Hypotonia, motor delay
Additional features Microcephaly	 Y	 Y	 Y	 Y (0.4^{th} – 2^{nd} percentile)	 Y (-0.5 SD)
Spasticity	Y	Y	Y	Y – LL>UL	Y
Seizures	N	Y – childhood onset	N	Y – now, resolved	N
Skin changes	Y – vitiligo	Y – vitiligo (progressive)	UK	Y – depigmented lesions	Y – depigmented lesions
Feeding difficulties	N	Y – NGT	N	Y – GOR	N
Other	Hypermobility, swan-neck deformity of fingers	Intermittent nystagmus, brisk DTRs	LL weakness, contractures	Central hypotonia, laryngomalacia, strabismus, small ASD, hypersensitivity to sounds	Central hypotonia
Development & progress Intellectual impairment	 Y – severe	 Y – severe	 Y – non-verbal	 Y	 Unk
Developmental delay	Y – severe	Y – severe	Y – speech and motor	Y – speech and motor	Y – speech and motor
Highest motor milestone	Commando crawls	Head control	Y – walks with significant support	Walked with support	Walked – unsteady
Developmental regression	N	Y – seizure onset in childhood	N	Y – no longer walks/crawls	N

	Family 4		Family 5	Family 6	Family 7
	P6	**P7**	**P8**	**P9**	**P10**
Variant 1; Variant 2	c.854-3A>G, p.(splice); c.854-3A>G, p.(splice)	c.854-3A>G, p.(splice); c.854-3A>G, p.(splice)	c.329G>A, p.Gly110Asp; c.329G>A, p.Gly110Asp	c.2215C>T, p.Gln739Ter; c.2215C>T, p.Gln739Ter	c.2215C>T, p.Gln739Ter; c.2215C>T, p.Gln739Ter
Presentation Age at onset Presenting features	 Birth Neonatal hypoglycaemia and thrombocytopenia	 Infant Acquired microcephaly, developmental delay	 Infant Hypotonia, areflexia, nystagmus	 Infant Global developmental delay	 Infant Global developmental delay
Additional features Microcephaly	 Y	 Y – acquired	 N	 Y	 Y
Spasticity	Y	Y	N	Y	Y
Seizures	Y - myoclonus	N	Y	N	N
Skin changes	*	*	N	N	N
Feeding difficulties	Y – PEG/J	*	Y	Y	Y
Other	Neonatal thrombocytopenia, hypoglycaemia, dyskinesia	Pre-term birth - chorioamnionitis	NA	Facial dysmorphism, axial hypotonia, retinal dystrophy	Ambiguous genitalia, failure to thrive
Development & progress Intellectual impairment	 Y – severe	 Y	 Y	 Y – severe	 Y – severe
Developmental delay	Y	Y – severe	Y	Y – severe	Y – severe
Highest motor milestone	*	*	Crawls	Walked with support	Sitting (supported)
Developmental regression	N	N	Y	Y – no longer mobile	N

	Family 8	Family 9
	P11	**P12**
Variant 1; Variant 2	c.1177G>A, p.Ala393Thr; c.1177G>A, p.Ala393Thr	c.196C>T, p.Pro66Leu; c.1240C>T, p.Pro414Ser
Presentation Age at onset Presenting features	 Birth Prenatal brain anomalies, neonatal respiratory distress	 Childhood Ataxia, encephalopathy, drooling, dystonia, dysarthria following viral illness.
Additional features Microcephaly	 Y	 N
Spasticity	Y	N
Seizures	Y – neonatal	N
Skin changes	Unk	N
Feeding difficulties	Y – NGT and GOR	N
Other	Lissencephaly, neonatal RDS	N
Development & progress Intellectual impairment	 Unk	 N
Developmental delay	Y	Y – mild
Highest motor milestone	Nil	Walking
Developmental regression	N	Y

For further clinical and demographic information about each patient, please contact the corresponding author.

Abbreviations: Y = yes; N = no; d = day; w = week; m = month; y = year; NA = not applicable; LL = lower limb; UL = upper limb; FTT = failure to thrive; Unk = unknown; ASD = atrial septal defect; PEG/J = percutaneous endoscopic gastro-jejunostomy, NGT = nasogastric tube, GOR = gastro-oesophageal reflux.

Supplementary Table 2: MRI features of patients with *SUPV3L1* variants

	P1	P2	P3	P4	P5	P6
Abnormal myelination						
Delayed	N	N	N	*	N	Y
Hypomyelination	Y	Y	Y	*	N	N
Dysmyelination	Y	Y	Y	*	Y	Y
Temporal horn changes	Y – SC cysts	Y – SC cysts	Y – SC cysts	Y – SC cysts	*	Y – SC cysts
Structural abnormality	*	*	*	Y – thin CC	Y – thin CC	N
Atrophy						
Cerebral	N	N	N	*	*	N
Cerebellar	Y	Y	Y	Y	Y - mild	N
Calcification	N	N	N	*	N	Y - BG
Other features	N	N	N	*	N	N

Abbreviations: Y = yes; N = no; m = month; y = year; CC = corpus callosum; SC = subcortical; BG = basal ganglia; * = unclear from available imaging

Supplementary Figure 1 – representative images from the optimisation and validation of the dsRNA complementation assay.

siRNA knockdown of SUPV3L1 results in an increase in double stranded RNA (dsRNA) that is not observed with the non-targeting siRNA. Subsequent transfection of wild-type SUPV3L1 leads to a reduction in dsRNA, suggestive of a rescue of the cellular phenotype. Transfection with a known mutation (p.Gln739Ter) did not show a corresponding rescue of the dsRNA levels to that of the wild-type. Scale bar represents 200µM.